

A $j_{\text{eff}}=1/2$ Kitaev material on the triangular lattice: The case of NaRuO_2

Aleksandar Razpopov,¹ David A. S. Kaib,¹ Steffen Backes,^{2,3,4} Leon Balents,⁵ Stephen D. Wilson,⁶ Francesco Ferrari,¹ Kira Riedl,¹ and Roser Valentí¹

¹*Institut für Theoretische Physik, Goethe-Universität, 60438 Frankfurt am Main, Germany*

²*Research Center for Advanced Science and Technology, University of Tokyo, Komaba, Tokyo 153-8904, Japan*

³*Center for Emergent Matter Science, RIKEN, Wako, Saitama 351-0198, Japan*

⁴*CPHT, CNRS, École polytechnique, Institut Polytechnique de Paris, 91120 Palaiseau, France*

⁵*Kavli Institute for Theoretical Physics, University of California, Santa Barbara, California 93106, USA*

⁶*Materials Department, University of California, Santa Barbara, California 93106-5050, USA*

(Dated: January 20, 2023)

Motivated by recent reports of a quantum disordered ground state in the triangular lattice compound NaRuO_2 , we derive a $j_{\text{eff}} = 1/2$ magnetic model for this system by means of first-principles calculations. The pseudospin Hamiltonian is dominated by bond-dependent off-diagonal Γ interactions, complemented by a ferromagnetic Heisenberg exchange and a notably *antiferromagnetic* Kitaev term. In addition to bilinear interactions, we find a sizable four-spin ring exchange contribution with a *strongly anisotropic* character, which has been so far overlooked when modeling Kitaev materials. The analysis of the magnetic model, based on the minimization of the classical energy and exact diagonalization of the quantum Hamiltonian, points toward the existence of a rather robust easy-plane ferromagnetic order, which cannot be easily destabilized by physically relevant perturbations.

INTRODUCTION

The first definition of a quantum spin liquid (QSL) state dates back to the milestone paper by P.W. Anderson in 1973 [1], in which the *resonating valence-bond* wave function, a macroscopic liquid-like superposition of singlet states, was proposed as a variational guess for the ground state of the triangular lattice Heisenberg antiferromagnet [2, 3]. Another archetypal portrait of a quantum spin liquid state is more recent and originated from the seminal work of A. Kitaev in 2006 [4], who set a bond-anisotropic spin model on the honeycomb lattice with an exact spin-liquid ground state represented in terms of Majorana fermions. Both these alternative descriptions of QSL states, which are associated to different microscopic mechanisms of frustration, left an indelible mark in the context of frustrated magnetism. On the one hand, the triangular lattice antiferromagnet is the prototypical example of a system with *geometric frustration*, where the presence of antiferromagnetic Heisenberg couplings over odd-sided loops of sites fights the tendency towards long-range magnetic order. On the other hand, the possibility of realizing *anisotropic interactions* as a consequence of the interplay between spin-orbit coupling (SOC), crystal field splitting and Hund's coupling [5–7] has opened a whole new field of investigation centered around the Kitaev materials [8, 9]. Even though the original Kitaev honeycomb model has no odd-sided loops and hence no geometric frustration, it nevertheless features *exchange frustration* [9, 10] due to the fact that bond-directional interactions with competing quantization axes cannot be satisfied simultaneously.

In this work, we investigate a recently synthesized compound, NaRuO_2 , in which both paradigms of magnetic

frustration described above come into play. The crystal structure of this material displays perfect triangular lattice planes of edge-sharing RuO_6 octahedra, separated by Na ions [11–13] (illustrated in Fig. 1). The same structural arrangement is found in a family of rare-earth chalcogenides which have been recently investigated as possible spin liquid candidates [14]: NaYbO_2 [15], NaYbS_2 [16, 17] and NaYbSe_2 [18]. However, at variance with the latter, the space group of NaRuO_2 is $R\bar{3}$ and, most importantly, the rare-earth ion is replaced by ruthenium, which belongs to the *d*-block of the periodic table. In analogy to the intensively studied honeycomb compound $\alpha\text{-RuCl}_3$ [8, 9], the strong spin-orbit coupling of ruthenium, combined with the geometry of edge-sharing ligand octahedra, is expected to realize a prime example for the Jackeli-Khaliullin mechanism to form a $j_{\text{eff}} = 1/2$ magnet with significant Kitaev interaction [7]. Resistivity measurements identified NaRuO_2 to be indeed insulating, with a small magnetization upon application of an external magnetic field, and a paramagnetic Curie temperature dependence of the magnetic susceptibility [12]. These signatures point toward the possibility of a QSL ground state, making a microscopically motivated magnetic model for NaRuO_2 not only intriguing, but also necessary.

The interplay between Heisenberg exchange and Kitaev interactions on the triangular lattice [19, 20] has been investigated in several works, revealing, for instance, the presence of crystals of \mathbb{Z}_2 vortices in proximity of the magnetic phase with 120° order [21], and possibly a spin nematic state around the antiferromagnetic Kitaev point [22–24]. Furthermore, an extended spin model featuring the Γ -exchange coupling [25], which can favor the onset of a stripy mag-

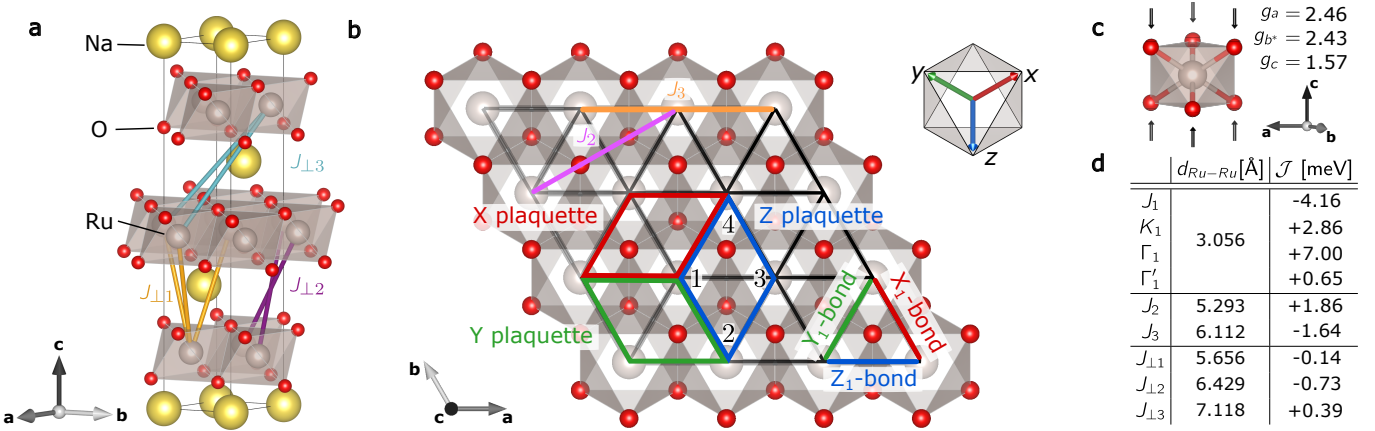


FIG. 1. **NaRuO₂ crystal structure, illustrations and DFT results for magnetic exchange parameters.** **a** Crystal structure of NaRuO₂ with illustration of interlayer bonds $J_{\perp i}$. **b** Top view of the triangular Ru lattice, with illustration of intralayer bonds and four-spin ring exchange plaquettes. The cubic coordinates employed in the magnetic model are oriented approximately along Ru-O bonds, as shown in the top right corner. **c** Trigonally compressed RuO₆ octahedron and corresponding *ab-initio* g -tensor values, with b^* defined perpendicular to the crystallographic a and c axes. **d** Magnetic exchange parameters for nearest neighbor (\mathcal{J}_1) and isotropic longer-range intra- (J_i) and interlayer ($J_{\perp i}$) bonds. The NN couplings, as defined in Eq. (1), are extracted with the projED method, while the isotropic J couplings are determined by TEMA within the VASP framework. The TEMA results are scaled by a factor of $J_1^{\text{projED}}/J_1^{\text{TEMA}} = 0.65$ (see main text).

netic phase, has been investigated in connection with the $j_{\text{eff}} = 1/2$ iridate compound Ba₃IrTi₂O₉ [26, 27]. In this regard, a comprehensive overview of the different phases induced by bond-anisotropic (nearest-neighbor) couplings on the triangular lattice is provided by Ref. [28]. More recently, analogous anisotropic spin Hamiltonians have been shown to capture the effective magnetic interactions of certain transition metal dihalides [29–31].

In addition to bilinear spin couplings, several magnetic materials with a triangular lattice structure, e.g. organic charge-transfer salts [32], are characterized by non-negligible four-spin ring exchange interactions [33], which incorporate higher order contributions in the perturbation-theory treatment of the Hubbard model around the Mott insulating regime. While at the (semi-)classical level ring-exchange can induce the formation of spirals and non-trivial chiral orders (e.g. spin-vortex crystals) [34], or significantly affect the low-energy magnon spectra of collinear phases [35], at the quantum level it is argued to potentially stabilize QSL phases [36, 37]; in this regard, the possible appearance of a gapless QSL with a spinon Fermi surface [38], or a Kalmeyer-Laughlin chiral state [39], has been discussed. An additional level of complication arises in magnetic systems with strong spin-orbit interactions, namely the presence of spin-anisotropic ring-exchange interactions, which have been scarcely investigated in the past [40].

In this work we perform a thorough inspection of the magnetic properties of NaRuO₂, from first-principles calculations to microscopic spin models. We provide theoretical justification for the low-energy description of NaRuO₂ in

terms of $j_{\text{eff}} = 1/2$ pseudospin degrees of freedom, highlighting the importance of different sources of interactions, such as intra- and inter-layer exchange couplings, and bond-anisotropic bilinear and ring-exchange interactions stemming from the strong spin-orbit coupling effects. The analysis of (classical and quantum) magnetic models indicate the existence of a robust easy-plane ferromagnetic (FM) order, which cannot be easily destabilized by perturbations around the *ab initio* derived spin Hamiltonian. Based on our proposed magnetic model, we also provide theoretical inelastic neutron scattering spectra, which can be directly compared to experiment.

RESULTS

Electronic properties

We begin by analyzing the electronic properties of NaRuO₂ with the help of density functional theory (DFT) calculations, as detailed in the Methods section. The octahedral environment of the Ru 4d⁵ sites leads to a crystal field splitting [8, 41, 42] with unoccupied e_g -states and occupied t_{2g} -states. The latter further split into $j_{\text{eff}} = 3/2$ and $j_{\text{eff}} = 1/2$ levels in the limit of strong spin-orbit coupling.

To estimate the Hubbard repulsion and Hund's coupling of NaRuO₂, we employ constrained random phase approximation (cRPA) calculations (see Methods section). In the non-relativistic band structure we observe a crossing between the Ru e_g band and a band with dominant Na 3s character close to the Γ point. This poses the question

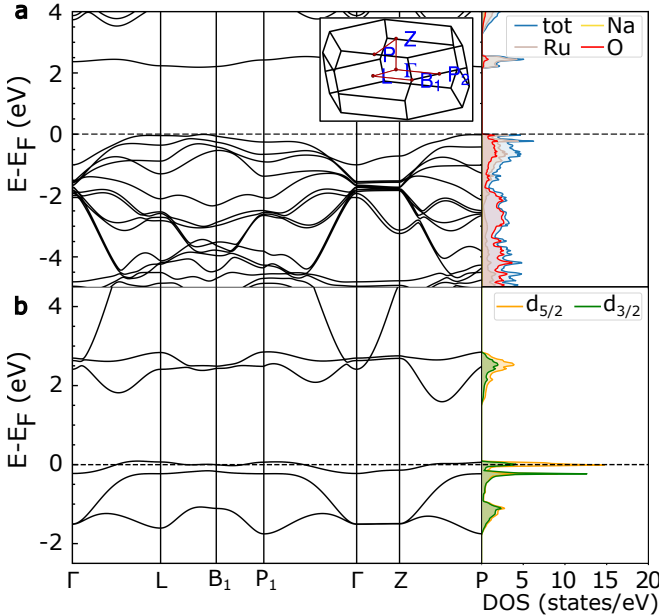


FIG. 2. Electronic band structure and density of states of NaRuO_2 . **a** Ferromagnetic GGA+SOC+U results, with $(U_{\text{avg}}, J_{\text{avg}}) = (3.15, 0.47)$ eV for the Ru 4d electrons, and magnetization polarized in the crystallographic a - b plane. **b** Non-magnetic GGA+SOC results. The partial DOS for Ru 4d orbitals displays a clear splitting of $j = 5/2$ and $j = 3/2$ weight.

about which bands should be included in the Wannierization procedure prior to cRPA. One option is considering only the five 4d Ru bands, which can be expected to lead to an artificially enhanced e_g screening. The corresponding cRPA result is $(U_{\text{avg}}, J_{\text{avg}})_{4d} = (3.114, 0.4736)$ eV. Alternatively, the crossing band may be included in a cRPA calculation based on a six-band model. This choice leads to an artificially suppressed screening, with $(U_{\text{avg}}, J_{\text{avg}})_{4d+3s} = (3.1865, 0.4756)$ eV. Since it turns out that both approaches lead to similar results, we choose to work with the average of them: $(U_{\text{avg}}, J_{\text{avg}}) = (3.15, 0.47)$ eV.

We employ these values as correlation corrections on the Ru 4d electrons in a relativistic band structure calculation (GGA+SOC+U, see Methods section) with ferromagnetically aligned magnetic moments. The resulting band structure and partial density of states (DOS) are shown in Fig. 2a. We choose the spin magnetic moments to be polarized in the crystallographic a - b plane, which is the most energetically favorable orientation. Within this setting we obtain an insulator with a charge gap of 2.1 eV which is in agreement with recent resistivity experiments [12]. We find that magnetism and Coulomb interaction are necessary to open a realistic charge gap in NaRuO_2 , which is further enlarged by SOC.

The partial DOS resolves the dominance of ruthenium weight around the Fermi level, such that we can proceed with a low-energy modelling of this compound based on

ruthenium bands.

The edge-sharing octahedral structure of NaRuO_2 hints towards the possibility of a $j_{\text{eff}} = 1/2$ description of the low-energy magnetic properties, in analogy with the intensively studied $\alpha\text{-RuCl}_3$ [8]. To check the validity of the relativistic j_{eff} picture for NaRuO_2 , we calculate also a non-magnetic band structure and a partial DOS resolved with respect to the general relativistic basis for d orbitals, $j = \{5/2, 3/2\}$ (shown in Fig. 2b). As detailed in Supplementary Note 1, the $j = 3/2$ states can be directly expressed as a sum of $j_{\text{eff}} = 3/2$ and e_g states. The information about the $j_{\text{eff}} = 1/2$ states on the other hand is contained in the $j = 5/2$ states. The small contribution of $j = 3/2$ states around the Fermi energy in Fig. 2b is thus an indication that a description in terms of pseudospin $j_{\text{eff}} = 1/2$ states is reasonable.

Magnetic Model

As an appropriate magnetic model for NaRuO_2 we consider a $j_{\text{eff}} = 1/2$ pseudospin Hamiltonian. To relate the pseudospin \mathbf{S} of the magnetic Hamiltonian to the magnetic moment, $\mathbf{M} = \mu_B \mathbb{G} \cdot \mathbf{S}$, we calculate the gyromagnetic g -tensor from first principles (see Methods section). We find it to be approximately diagonal with $(g_a, g_{b^*}, g_c) = (2.46, 2.43, 1.57)$ in crystallographic coordinates (with b^* perpendicular to a and c). With respect to the triangular plane, the in-plane components (g_a, g_{b^*}) are larger than the out-of-plane one (g_c), as a direct consequence of the trigonal compression of the RuO_6 octahedra along the crystallographic c axis (see Fig. 1c) [43].

For the magnetic interactions between the pseudospins we consider a Hamiltonian consisting of a bilinear exchange term \mathcal{H}_2 and a four-spin ring exchange term \mathcal{H}_4 . We express this model in the conventionally used cubic coordinates for Kitaev materials, which consist of orthogonalized axes oriented approximately along the Ru-O bonds, as illustrated in the top right corner of Fig. 1b. We denote the three components of the pseudospin at site i as S_i^μ , with $\mu = \{x, y, z\}$. In this framework, the [111] pseudospin direction is parallel to the crystallographic c axis. For completion, in Supplementary Note 2 we translate our model to an alternative reference frame with crystallographic coordinates [28]. The bilinear contribution to the magnetic Hamiltonian $\mathcal{H}_2 = \sum_{i < j} \sum_{\mu\nu} \mathbb{J}_{ij}^{\mu\nu} S_i^\mu S_j^\nu$ contains, especially for nearest neighbors, anisotropic bond-dependent terms. Considering the symmetry constraints of the $\bar{R}\bar{3}$ space group, the bilinear exchange tensor on a Z_1 -bond (as defined in Fig. 1b) follows the form

$$\mathbb{J}_{Z_1\text{-bond}} = \begin{pmatrix} J_1 & \Gamma_1 & \Gamma'_1 \\ \Gamma_1 & J & \Gamma'_1 \\ \Gamma'_1 & \Gamma'_1 & J_1 + K_1 \end{pmatrix}. \quad (1)$$

Here, J_1 is the isotropic Heisenberg exchange, K_1 the Kitaev coupling, and Γ_1 and Γ'_1 the off-diagonal symmetric

exchange parameters. The bilinear interactions on X_1 - and Y_1 -bonds are then related to this expression by C_3 spin rotations around the [111] axis, amounting to cyclic permutation of (x, y, z) spin components.

We performed DFT calculations to obtain the magnetic exchange parameters as described in the Methods section. In Fig. 1d we show the dominant magnetic couplings extracted for nearest-neighbor bonds with the projED method [44] and the isotropic longer-range exchange from total energy mapping analysis (TEMA). Both methods predict similarly strong intralayer ferromagnetic Heisenberg J_1 coupling, when we consider a scaling factor $J_1^{\text{projED}}/J_1^{\text{TEMA}} \approx 0.65$. The shortest further-neighbor intralayer couplings are found to be non-negligible and of similar magnitude, with J_2 being anti- and J_3 ferromagnetic. The interlayer Heisenberg couplings $J_{\perp 1}$, $J_{\perp 2}$ and $J_{\perp 3}$ (shown in Fig. 1a) are one magnitude smaller than the intralayer ones, with $J_{\perp 1}$ and $J_{\perp 2}$ being ferromagnetic and $J_{\perp 3}$ antiferromagnetic.

Within the projED method we obtain the bond-dependent anisotropic couplings K_1 , Γ_1 and Γ'_1 at nearest-neighbors, where the cRPA values $(U_{\text{avg}}, J_{\text{avg}}) = (3.15, 0.47)$ eV are employed. Compared to previously estimated magnetic parameters for other Ru 4d systems [45–48], it is interesting to note that we have strongly *antiferromagnetic* Kitaev K_1 term and a dominant positive Γ_1 as the largest coupling. These are contributions which, to the best of our knowledge, have not been observed in a real material with effective spin 1/2 so far.

The microscopic origin of the unusual antiferromagnetic sign of the Kitaev interaction encountered here can be understood as follows: From the perspective of second-order perturbation theory in a perfect octahedral environment (considering only the occupied t_{2g} orbitals), the Kitaev interaction scales as $K_1 \propto (t_1 - t_3)^2 - 3t_2^2$ [49]. On a Z-bond, the hopping parameters are defined as the ligand-assisted hopping $t_2 = t_{(xz;yz)}$, as well as $t_1 = t_{(xz;xz)} = t_{(yz;yz)}$ and $t_3 = t_{(xy;xy)}$, which stem predominantly from direct d orbital overlap. For the prime example of the honeycomb Kitaev material $\alpha\text{-RuCl}_3$, the indirect hopping t_2 is dominant, somewhat close to the t_2 -only model in the Jackeli-Khaliullin mechanism, where the Kitaev interaction is ferromagnetic ($K_1 \propto -3t_2^2$) [7]. In comparison, the direct hoppings t_3 and t_1 gain importance in NaRuO_2 , where the nearest neighbor Ru-Ru bond length is significantly smaller than in $\alpha\text{-RuCl}_3$. As dictated by the geometry, t_3 is negative and larger in magnitude than the positive t_1 . The resulting *antiferromagnetic* Kitaev interaction in NaRuO_2 can hence be directly related to the shorter nearest-neighbor bond length of this triangular compound. The perturbation theory perspective also offers an explanation for the dominance of the off-diagonal symmetric exchange Γ_1 , which scales approximately as $\Gamma_1 \propto t_2(t_1 - t_3)$ [49]. While the magnitude of K_1 reduces with the competition between in-

direct and direct contributions, Γ_1 increases proportional to the magnitude of the hoppings, leading to a magnetic model dominated by the off-diagonal symmetric exchange for NaRuO_2 .

Despite the antiferromagnetic sign of the Kitaev interaction, the bilinear exchange Hamiltonian \mathcal{H}_2 features a ferromagnetically ordered ground state, due to significant $J_1 < 0$ and $\Gamma_1 > 0$ interactions, as discussed in more detail below. To seek out possible additional interactions that might destabilize the ferromagnetic ground state, we consider the effects of higher-order ring exchange interactions. Compared to honeycomb Kitaev materials, NaRuO_2 could be predestined for such interactions, due to the marginally insulating Mott state reported in experiments [12] and to its triangular lattice structure, where the shortest closed loops consist of four (instead of six) sites. Four-spin ring exchange without spin-orbit coupling effects has been discussed plentifully in the literature [33, 35–37, 39] and takes the form

$$\mathcal{H}_4^{\text{iso}} = \frac{K^{\text{iso}}}{S^2} \sum_{\langle ijk \rangle} (\mathbf{S}_i \cdot \mathbf{S}_j)(\mathbf{S}_k \cdot \mathbf{S}_l) + (\mathbf{S}_i \cdot \mathbf{S}_l)(\mathbf{S}_j \cdot \mathbf{S}_k) - (\mathbf{S}_i \cdot \mathbf{S}_k)(\mathbf{S}_j \cdot \mathbf{S}_l), \quad (2)$$

where the summation $\langle ijk \rangle$ goes over plaquettes with sites i and k lying across a diagonal [33], K^{iso} is the coupling constant, and the superscript “iso” denotes that this is the conventional isotropic (i.e., SU(2)-symmetric) ring exchange. However, for NaRuO_2 there is no reason why the ring exchange between the pseudospin $j_{\text{eff}} = \frac{1}{2}$ moments should follow the form of $\mathcal{H}_4^{\text{iso}}$, since spin-orbit coupling is expected to induce anisotropic four-site terms in the Hamiltonian. In the most general form, anisotropic four-spin exchange may be expressed as

$$\mathcal{H}_4^{\text{tot}} = \frac{1}{S^2} \sum_{\langle ijk \rangle} \sum_{\mu\nu\rho\eta} \mathbb{K}_{ijkl}^{\mu\nu\rho\eta} (S_i^\mu S_j^\nu S_k^\rho S_l^\eta), \quad (3)$$

where the tensor \mathbb{K} contains the coupling constants. The presence of inversion symmetry with respect to the center of each plaquette, together with a C_2 rotation axis parallel to the shortest diagonal, reduces the 81 entries of \mathbb{K} for one plaquette to 24 independent parameters. Furthermore, analogous to the X-, Y-, and Z-bonds of bilinear exchange, it is convenient to define X-, Y-, and Z-plaquettes, as shown in Fig. 1b. The three plaquettes are related by C_3 rotations around the out-of-plane axis and hence the tensor of one plaquette type fully encodes $\mathcal{H}_4^{\text{tot}}$.

Note that in contrast to conventional ring exchange, care has to be taken for the order of the site-numbering within a plaquette. For example, for a single plaquette (with the site labeling illustrated in Fig. 1b), swapping two sites across a diagonal is not a symmetry of the ring-exchange tensor, i.e. $\mathbb{K}_{1234}^{\mu\nu\rho\eta} \neq \mathbb{K}_{1432}^{\mu\nu\rho\eta}$, even in presence of the aforementioned symmetries.

To compute the ring-exchange tensor \mathbb{K} from first principles, we employ the projED method, which has been used previously to determine ring-exchange couplings for organic triangular lattice compounds [34, 50]. Results on a Z-plaquette are given in Table I, and details of the calculation are outlined in the Methods section. We do not attempt to create a minimal model here and show agnostically the full *ab-initio* result. Overall, the four-site ring exchange contribution in NaRuO_2 does not seem to be obviously negligible, with a strength of roughly 5-10% of the nearest-neighbor bilinear exchange parameters. As anticipated, the shown results deviate substantially from the conventional isotropic ring exchange $\mathcal{H}_4^{\text{iso}}$. This is not surprising because of the strong spin-orbit coupling in NaRuO_2 . For instance, among the diagonal components characterizing the Z-plaquette, the $\mathbb{K}_{1234}^{\text{zzzz}}$ term strongly differs from $\mathbb{K}_{1234}^{\text{xxxx}} = \mathbb{K}_{1234}^{\text{yyyy}}$.

To quantify the degree of anisotropy of the total ring exchange Hamiltonian encoded in Table I, we express it as a sum consisting of the conventional isotropic ring exchange from Eq. (2) and a purely anisotropic contribution: $\mathbb{K}^{\text{tot}} = \mathbb{K}^{\text{iso}} + \mathbb{K}^{\text{ani}}$. The choice of this splitting is not unique, but we choose the coupling constant K^{iso} in $(\mathbb{K}^{\text{iso}})_{1234}^{\mu\nu\rho\eta} = K^{\text{iso}} (\delta_{\mu\nu}\delta_{\rho\eta} + \delta_{\mu\eta}\delta_{\nu\rho} - \delta_{\mu\rho}\delta_{\nu\eta})$ (cf. Eq. (2)) such that the tensor-norm of the anisotropic part, $\|\mathbb{K}^{\text{ani}}\| = \|\mathbb{K}^{\text{tot}} - \mathbb{K}^{\text{iso}}\|$, is minimized. Here, the tensor 1-norm is used ($\|\mathbb{K}\| = \sum_{\mu\nu\rho\eta} |\mathbb{K}_{1234}^{\mu\nu\rho\eta}|$). This choice is motivated by an analogy to the case of the bilinear Hamiltonian, where the same procedure splits the bilinear exchange tensor $\mathbb{J}_{ij}^{\mu\nu}$ into an (isotropic) Heisenberg exchange part and an anisotropic part, arriving at the same definition of Heisenberg- J as in Eq. (1). Dissecting the ring exchange interaction in this way leads to $K^{\text{iso}} = -0.06 \text{ meV}$ and $\|\mathbb{K}^{\text{ani}}\| / \|\mathbb{K}^{\text{iso}}\| = 5.6$, which shows that ring exchange in NaRuO_2 is dominated by the anisotropic contributions.

Properties of the Magnetic Model

We investigate the ground state of the magnetic model given in Fig. 1d by applying two different methods. We consider the classical ground state via an iterative minimization method of the energy [51, 52] and then we include quantum fluctuations by tackling the Hamiltonian with exact diagonalization (ED) on finite clusters with up to 27 sites (see Methods section and Supplementary Note 3).

First we consider the classical ground state of the \mathcal{H}_2 Hamiltonian restricted to the triangular lattice plane. The omission of inter-layer couplings is justified by their small estimated magnitude compared to intra-layer couplings (cf. Fig. 1d). The minimum of the classical energy is provided by a ferromagnetic spin arrangement, with spins lying in the triangular lattice plane. The ferromagnetic nature of the ground state turns out to be stable upon different perturbations of the Hamiltonian around the *ab initio* model (as discussed in Supplementary Note 4), and upon inclusion of anisotropic ring exchange or out-of-plane interac-

$\mathbb{K}_{1234}^{\mu\nu\rho\eta} [\text{meV}]$	$S_1^\mu S_2^\nu S_3^\rho S_4^\eta$
0.1829	(xxzx + yyzy + zxxx + zyyy)
0.1828	(xxzy + yxzy + zyxx + zyyx)
0.1819	(zxzy + zyzx)
0.1810	(xzyz + yzxz)
-0.1740	(zzzz)
-0.1559	(xyzz + yzzx + zxyz + zzxy)
-0.1457	(xzzx + yyzz + zxzx + zzyy)
-0.1398	(xxxx + yyyy)
-0.1284	(xxxx + xzxx + yyyy + yzyy)
0.1122	(zxzz + zyzz + zzzx + zzzy)
-0.0969	(xyxy + yxyx)
-0.0829	(xyzy + yxzx + zxyx + zyxy)
0.0602	(xyzx + yyzx + zxxy + zxxy)
-0.0596	(xyxz + xzxy + yxyz + yzyx)
-0.0581	(xzzz + yzzz + zzzx + zzyz)
-0.0580	(xxzz + yzzy + zyyz + zzxx)
-0.0570	(xzyx + xzyy + yxxz + yyxz)
-0.0542	(xxxx + xyxx + yxxy + yyyx)
0.0354	(xxyz + xyyz + yzxx + yzxy)
-0.0352	(xzzy + yxzz + zyxz + zzyx)
-0.0272	(xxyy + xyyx + yxxx + yyxx)
0.0252	(zxzx + yzyz)
0.0145	(xxyx + xyyy + yxxx + yyxy)
0.0069	(zxzx + zyzy)

TABLE I. **Four-spin ring exchange couplings for NaRuO_2 .** The corresponding ring-exchange expression is defined in Eq. (3) and the parameters in this table refer to a Z-plaquette, with the site labeling 1, 2, 3, 4 illustrated in Fig. 1b. The ring-exchange parameters are calculated with projED starting from a three-orbital Hubbard model. For simplicity, we abbreviate $S_1^\mu S_2^\nu S_3^\rho S_4^\eta$ with “ $\mu\nu\rho\eta$ ”. Parameters for X- and Y-plaquettes follow by C_3 rotations around the out-of-plane axis.

tions. For what concerns the latter, the classical energy minimum yields a ferromagnetic ground state, with spins being parallel to each other both within and between layers, consistent with total energy calculations within DFT. However, the configuration with ferromagnetically stacked FM layers is lower in energy than the one with antiferromagnetically stacked FM layers only by $\sim 0.1 \text{ meV/Ru}$. ED calculations, performed on various two-dimensional clusters with different shapes and number of sites, confirm the stability of the ferromagnetic ground state when quantum effects come into play. The addition of the ring-exchange interaction $\mathcal{H}_4^{\text{tot}}$ does not destabilize the ferromagnetic order, neither for classical nor for quantum spins, but leads to a small tilt of the ordered moment out of the triangular lattice plane (by less than 1° in our model).

After having established the ferromagnetic character of the ground state, we move on to compute excitations, namely the inelastic neutron scattering (INS) intensity predicted by the magnetic model. We employ linear spin-wave theory (LSWT), complemented by ED to investigate effects beyond LSWT. The results are summarized in Fig. 3, where the

ab initio magnetic form factor for Ru^{3+} [53] is taken into account for the calculation of spectral intensities, such that the magnetic spectra can be directly compared to neutron scattering experiments.

As previously mentioned, the magnetic moments of the ferromagnetic ground state of the \mathcal{H}_2 Hamiltonian lie within the triangular lattice plane, without picking any preferred direction on the classical level. However, this continuous symmetry is accidental and is lifted by quantum fluctuations, which select the configurations in which the moments are perpendicular to one of the nearest-neighbor bonds [28]. At the *linear* spin wave theory level we then expect the appearance of a gapless pseudo-Goldstone mode, which becomes gapped when quantum effects beyond the lowest-order are considered [54]. The ED results, compared to the LSWT prediction in Fig. 3b, confirm this picture, and find a gap at $\mathbf{q} = 0$ of the order of 1 to 2 meV.

A further effect beyond LSWT that one might expect here is the appearance of strong scattering continua even in magnetically ordered phases. Such continua were observed in the honeycomb Kitaev material $\alpha\text{-RuCl}_3$ [55], where they have been traced back in a spin-wave description to originate from significant anharmonic effects due to Γ_1 exchange [45]. However, despite the dominant off-diagonal Γ_1 exchange in the case of NaRuO_2 (cf. Fig. 1d), no substantial scattering continuum is found here and the ED spectrum qualitatively follows the sharp modes of LSWT, as shown in a comparison in Fig. 3b. This can be understood as a consequence of the fact that in the present ferromagnetic state, the pseudo-Goldstone modes remain at the ordering-wave vector $\mathbf{Q} = 0$ (Γ -point), such that a potential decay of single-magnons into a two-magnon continuum via Γ_1 -exchange is kinematically not allowed. We note that the inclusion of ring exchange increases the magnon energies by ~ 2 meV, but does not qualitatively change the main features of the spectrum.

We also compute the powder-averaged INS spectrum that might be relevant for direct comparison of the predicted FM state to experiments. Here, the effect of inter-plane couplings are included, in order to obtain meaningful integration over out-of-plane momenta. The results from LSWT are shown in Fig. 3c and feature the gapless pseudo-Goldstone mode at smallest momenta, and a less intense gapless mode around 1.2 \AA^{-1} arising from the inter-layer ferromagnetic stacking.

Conclusions and Outlook

In this work we investigated the magnetic properties of NaRuO_2 , a layered system of corner-sharing RuO_6 octahedra, which constitutes a prime example for the realization of anisotropic spin couplings, such as the Kitaev interaction, on a triangular lattice structure. By combining two complementary first-principle methods, TEMA and projED, we derived a $j_{\text{eff}} = 1/2$ pseudospin Hamiltonian for NaRuO_2 ,

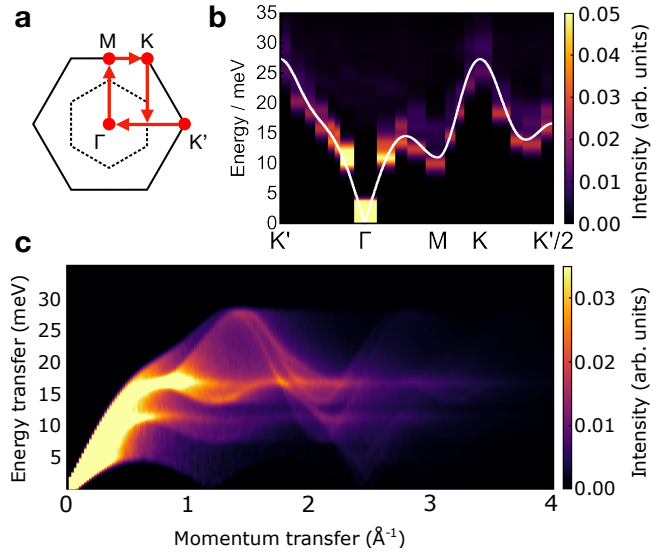


FIG. 3. Computed neutron scattering intensity within the magnetic model. **a** Momentum path in the Brillouin zone of the triangular lattice, **b** INS intensity for the Hamiltonian \mathcal{H}_2 without inter-plane interactions, along high-symmetry lines in momentum space. Color plot intensity from ED (with a broadening of 1 meV), combined from different clusters from 18 to 27 sites. The overlayed band dispersion is the single-magnon energy from LSWT. As the ED ground state is a superposition of different degenerate magnetic domains, the compared LSWT energy is plotted as the average of three calculations, which correspond to expansions around in-plane ferromagnetic order, with magnetic moments perpendicular to X_1 -, Y_1 - or Z_1 -bonds. **c** Calculated powder-averaged INS spectrum, from the model in Fig. 1d, including inter-plane exchange couplings. Note that (different) arbitrary units are used for the intensities in **b** and **c**, with cut-offs due to large intensity at $\mathbf{q} \approx 0$.

which displays a sizable *antiferromagnetic* Kitaev coupling. This is a direct consequence of the comparatively smaller nearest-neighbor Ru - Ru bond length in NaRuO_2 , leading to a dominance of direct hopping mechanisms in contrast to other spin-1/2 Kitaev materials to date. The strongest interactions of the model are however a symmetric Γ_1 exchange and a ferromagnetic J_1 Heisenberg term. The spin Hamiltonian with bilinear interactions possesses a rather robust ferromagnetic order, oriented parallel to the triangular lattice plane formed by ruthenium ions, also when longer-range intra- and inter-plane exchange interactions are taken into account.

The parameters of the magnetic Hamiltonian, as obtained by first-principles calculations with the pristine structure of NaRuO_2 , place this material deep inside an extended ferromagnetic phase, which cannot be easily destabilized by perturbing the Hamiltonian around the *ab initio* point. Since the experimentally available results do not show the conventional features of long-range ferromagnetic order and suggest the possibility of a marginally insulating Mott state

in NaRuO_2 [12], we explored the effects of higher-order spin interactions, computing four-spin ring exchange couplings from the projED method. However, although the latter turn out to be of non-negligible size, they seem insufficiently strong to melt the ferromagnetic order. Nevertheless, the nature of the ring exchange interaction is strongly anisotropic and its consequences warrant further investigation, also in the context of other Kitaev materials.

Furthermore, employing LSWT calculations and exact diagonalization on finite clusters, we computed the inelastic neutron scattering spectra for NaRuO_2 . Comparison of the powder-average neutron scattering intensity with experimental observations shows a similar weight distribution which may signal the presence of underlying ferromagnetism in the system, although no long-range magnetic order was observed in experiments [12, 13]. This raises the question of the role of disorder in the material, which may be addressed in future investigations.

Note added

During the process of completion of this manuscript, we became aware of the preprint [56], which provides a nearest-neighbor spin Hamiltonian for NaRuO_2 from quantum chemistry methods. While the signs of the nearest-neighbor couplings match with the ones of our model, the Γ_1 term of Ref. [56] is smaller than the J_1 exchange strength, contrary to our results. The authors explore the possibility of destabilizing the ferromagnetic order by an antiferromagnetic third-neighbors exchange, which is in contrast with our first-principle prediction of a ferromagnetic J_3 coupling.

METHODS

First principles calculations

All first principles calculations employ the crystal structure published in Ref. [12]. For the calculation of electronic properties we use the full potential local orbital (FPLO) [57] package 18.00-57 and the Generalized Gradient Approximation (GGA) [58] as the exchange-correlation functional. The correlation for the strongly localized Ru 4d electrons are corrected via the GGA+U approximation using the “atomic limit” implementation [59]. All calculations are carried out on a $12 \times 12 \times 12$ k-grid in the primitive unit cell. Relativistic calculations are performed within the GGA+SOC+U functional. The results have been cross-checked with the linearized augmented plane-wave basis set as implemented in Wien2k [60] version 19.1, with Ru 4d correlation correction included via the SIC method [61, 62] with effective Coulomb repulsion $U_{\text{eff}} = 2$ eV.

We also compute the gyromagnetic g -tensor from first principles. For this calculation, we consider a $[\text{RuO}_6]^{9-}$ molecule within the quantum chemistry ORCA 5.03 package [63] with the functional TPSSh, basis set def2-TZVP

and complete active space self-consistent field method for the d orbitals CASSCF(5,5). A conductor-like polarizable continuum model (C-PCM) [64] is employed with a Gaussian charge scheme, a van der Waals-type cavity and an infinite dielectric constant.

Constrained random phase approximation (cRPA)

Based on the electronic structure obtained with the Wien2k package v21.1 [60] we estimate the electronic two-particle interaction terms in NaRuO_2 with the constrained random-phase approximation (cRPA) [65, 66], as implemented in the FHI-gap code [67]. The integration of the Brillouin zone is done on an $8 \times 8 \times 8$ grid. The static low-energy limit of the partially screened interaction is projected onto the relevant orbitals, where screening processes in the same window are excluded. The spherical symmetric expressions for d electrons in the atomic limit are based on Slater integrals F_k [62] as follows:

$$U_{\text{avg}} = \frac{1}{(2l+1)^2} \sum_{\alpha\beta} U_{\alpha\beta} = F_0 \quad (4)$$

$$J_{\text{avg}} = \frac{7}{5} \frac{1}{2l(l+1)} \sum_{\alpha\neq\beta} J_{\alpha\beta} = \frac{F_2 + F_4}{14}, \quad (5)$$

where α, β are orbital indices and l is the angular momentum quantum number.

As mentioned in the Results section, due to a band crossing of the Ru e_g bands with a Na 3s band in NaRuO_2 , there are two sensible ways to select the relevant orbitals considered in the Wannier projection. We denote results based on the five Ru 4d orbitals as $(U_{\text{avg}}, J_{\text{avg}})_{4d}$ and results including also the Na 3s band as $(U_{\text{avg}}, J_{\text{avg}})_{4d+3s}$. Since both these options lead to very similar results, further calculations in the main text adopt the average of both cRPA results.

DFT-based derivation of the magnetic model

We extract the dominant magnetic Heisenberg couplings via the total energy mapping analysis (TEMA) [68–70], which is a two step process. First, we calculate total energies within DFT (GGA+U) of different magnetic configurations of chosen supercells of NaRuO_2 . In the second step we fit the DFT energy of the different magnetic configurations to an effective Heisenberg spin-1/2 Hamiltonian using the method of least squares. The first step is performed in the VASP 5.3 framework [71] using spin-polarized DFT+U, where we apply the Dudarev scheme [72], with effective Coulomb repulsion $U_{\text{eff}} = 3.5$ eV. Here, we consider 14 different magnetic configurations. The calculations are performed within a $3 \times 2 \times 1$ super cell on $5 \times 8 \times 3$ Γ -centered k-grid with energy cut-off of 540 eV for the plane-wave basis set. The quality of the total energy mapping analysis for the considered model is discussed in Supplementary Note 5. We have checked that different values of the effective Coulomb repulsion don't significantly affect the ratio between the various

exchange couplings.

As a second method we employ the so-called projED technique [44]. The approach consists of two main steps. First, an effective $4d$ electronic Hamiltonian $\mathcal{H}_{\text{tot}} = \mathcal{H}_{\text{hop}} + \mathcal{H}_{\text{U}}$ is constructed, where \mathcal{H}_{hop} consists of complex electronic hopping parameters, determined from first principles via Wannier projection of a relativistic band structure calculation (GGA+SOC). Here, we extract the Wannier functions by using the full potential local orbital (FPLO) [57] package 18.00-57. \mathcal{H}_{U} contains the electronic two-particle Coulomb interaction [44]. In a second step, the electronic Hamiltonian is solved by exact diagonalization on a two-site five-orbital cluster and its low energy states are projected onto spin operators, arriving at the desired effective spin Hamiltonian, e.g. $\mathcal{H}_2 = \mathbb{P}\mathcal{H}_{\text{tot}}\mathbb{P} = \sum_{i < j} \sum_{\mu\nu} \mathbb{J}_{i,j}^{\mu\nu} S_i^\mu S_j^\nu$. Note that here \mathbf{S} is a pseudospin with $j_{\text{eff}} = 1/2$. We employ the projED method for the calculation of nearest-neighbor couplings, while for longer-range interactions we resort to TEMA results. This choice is motivated by the fact that, within projED, the indirect hoppings over multiple sites, which are expected to become more and more important for longer-range couplings, cannot be accounted for due to computational limitations.

We also employ the projED method to extract the four-spin ring exchange Hamiltonian $\mathcal{H}_4^{\text{tot}}$. Due to computational limitations, the parameters are extracted by diagonalizing a four-site three-orbital electronic Hamiltonian involving only Ru t_{2g} orbitals. We adopt this approximation since the aim of this work is to estimate the general form and order of magnitude of the ring exchange interaction in a strongly spin-orbit coupled system like NaRuO₂. Possible refinements of this approach are beyond the scope of this work and will be pursued in future studies.

Iterative minimization (classical spins)

We obtain the classical ground state of the spin Hamiltonian \mathcal{H} by performing a numerical minimization of the energy on a finite lattice with periodic boundary conditions. We employ an *iterative method* in which the orientation of the spins (unit vectors at the classical level) is initialized with random values and updated by performing local moves. A single update is performed by selecting a random site i and changing its spin orientation according to

$$\mathbf{S}_i \mapsto -\frac{\mathbf{h}_i}{\|\mathbf{h}_i\|} \quad \text{where} \quad \mathbf{h}_i = \left(\frac{\partial \mathcal{H}}{\partial S_i^x}, \frac{\partial \mathcal{H}}{\partial S_i^y}, \frac{\partial \mathcal{H}}{\partial S_i^z} \right). \quad (6)$$

In other words, we anti-align the spin at site i to the effective field \mathbf{h}_i created by the interactions with the other spins in the lattice. The procedure is repeated several times until the minimum of the energy is reached. To try mitigating the

possibility of ending up in local energy minima, we perform a number of different calculations starting from different random initializations. Most numerical results have been obtained on a triangular lattice of $N = 12 \times 12 = 144$ sites. For calculations involving inter-layer couplings we used a three-dimensional cluster of $N = 6 \times 6 \times 6 = 216$ sites.

Exact diagonalization

We perform exact diagonalization of the $j_{\text{eff}} = 1/2$ model on two-dimensional clusters of up to $N = 27$ sites. The inelastic neutron scattering intensity at momentum \mathbf{k} and energy ω is given by

$$\mathcal{I}(\mathbf{k}, \omega) \propto f^2(k) \int dt e^{-i\omega t} \sum_{\mu, \nu} \left(\delta_{\mu, \nu} - \frac{k_\mu k_\nu}{k^2} \right) \langle S_{-\mathbf{k}}^\mu(t) S_{\mathbf{k}}^\nu(0) \rangle \quad (7)$$

where $f(k)$ is the atomic form factor of Ru³⁺. To compute it, we employ the continued fraction method and show results with a Gaussian pole broadening of $\sigma = 1$ meV. To access a higher number of \mathbf{k} -points, we plot together results coming from clusters of different shapes and sizes up to $N = 27$ (clusters shown in Supplementary Note 3), similar to as done in e.g. Ref. [45].

Linear spin-wave theory

Linear spin-wave theory calculations are performed with the SpinW 3.0 library [73]. The inelastic neutron scattering intensity is computed by taking the powder-average of Eq. (7).

ACKNOWLEDGEMENTS

We thank V. Krewald and I. I. Mazin for valuable advice regarding the *ab initio* calculations. We thank also D. Ceresoli, M. Imada, J. Kuneš and P.A. Maksimov for fruitful comments and discussions. R.V., A.R., K.R., D.A.S.K. and F.F. gratefully acknowledge support by the Deutsche Forschungsgemeinschaft (DFG, German Research Foundation) for funding through Project No. 411289067 (VA117/15-1), TRR 288 — 422213477 (project A05) and CRC 1487 - 443703006 (project A01). L.B. was supported by the DOE, Office of Science, Basic Energy Sciences under Award No. DE-FG02-08ER46524. S.D.W. acknowledges support by DOE, Office of Science, Basic Energy Sciences under Award No. DE-SC0017752.

AUTHOR CONTRIBUTIONS

R.V., S.D.W. and L.B. conceived the project. Density functional theory calculations were performed by A.R., K.R., cRPA calculations by S.B., projED calculations by K.R. and calculations on magnetic models by D.A.S.K. and F.F. All authors contributed to the writing of the manuscript.

[1] P. Anderson, *Mater. Res. Bull.* **8**, 153 (1973).

[2] P. Fazekas and P. W. Anderson, *Philos. Mag.* **30**, 423 (1974).

[3] L. Balents, *Nature* **464**, 199 (2010).

[4] A. Kitaev, *Annals of Physics* **321**, 2 (2006).

[5] G. Khaliullin, W. Koshibae, and S. Maekawa, *Phys. Rev. Lett.* **93**, 176401 (2004).

[6] G. Khaliullin, *Prog. Theor. Phys.* **160**, 155 (2005).

[7] G. Jackeli and G. Khaliullin, *Phys. Rev. Lett.* **102**, 017205 (2009).

[8] S. M. Winter, A. A. Tsirlin, M. Daghofer, J. van den Brink, Y. Singh, P. Gegenwart, and R. Valentí, *J. Phys. Condens. Matter* **29**, 493002 (2017).

[9] S. Trebst and C. Hickey, *Phys. Rep.* **950**, 1 (2022).

[10] L. Janssen and M. Vojta, *J. Phys. Condens. Matter* **31**, 423002 (2019).

[11] M. Shikano, C. Delmas, and J. Darriet, *Inorg.* **43**, 1214 (2004).

[12] B. Ortiz, P. Sarte, A. H. Avidor, A. Hay, E. Kenney, A. Kolesnikov, A. Aczel, C. Brown, C. Wang, M. Graf, R. Seshadri, L. Balents, and S. Wilson, *Preprint available at Research Square* (2022).

[13] B. R. Ortiz, P. M. Sarte, A. H. Avidor, and S. D. Wilson, *Phys. Rev. Mater.* **6**, 104413 (2022).

[14] W. Liu, Z. Zhang, J. Ji, Y. Liu, J. Li, X. Wang, H. Lei, G. Chen, and Q. Zhang, *Chin. Phys. Lett.* **35**, 117501 (2018).

[15] M. M. Bordelon, E. Kenney, C. Liu, T. Hogan, L. Posthuma, M. Kavand, Y. Lyu, M. Sherwin, N. P. Butch, C. Brown, M. J. Graf, L. Balents, and S. D. Wilson, *Nat. Phys.* **15**, 1058 (2019).

[16] M. Baenitz, P. Schlender, J. Sichelschmidt, Y. A. Onykiienko, Z. Zangeneh, K. M. Ranjith, R. Sarkar, L. Hozoi, H. C. Walker, J.-C. Orain, H. Yasuoka, J. van den Brink, H. H. Klauss, D. S. Inosov, and T. Doert, *Phys. Rev. B* **98**, 220409 (2018).

[17] R. Sarkar, P. Schlender, V. Grinenko, E. Haeussler, P. J. Baker, T. Doert, and H.-H. Klauss, *Phys. Rev. B* **100**, 241116 (2019).

[18] P.-L. Dai, G. Zhang, Y. Xie, C. Duan, Y. Gao, Z. Zhu, E. Feng, Z. Tao, C.-L. Huang, H. Cao, A. Podlesnyak, G. E. Granroth, M. S. Everett, J. C. Neufeind, D. Voneshen, S. Wang, G. Tan, E. Morosan, X. Wang, H.-Q. Lin, L. Shu, G. Chen, Y. Guo, X. Lu, and P. Dai, *Phys. Rev. X* **11**, 021044 (2021).

[19] I. Kimchi and A. Vishwanath, *Phys. Rev. B* **89**, 014414 (2014).

[20] G. Jackeli and A. Avella, *Phys. Rev. B* **92**, 184416 (2015).

[21] I. Rousochatzakis, U. K. Rössler, J. van den Brink, and M. Daghofer, *Phys. Rev. B* **93**, 104417 (2016).

[22] M. Becker, M. Hermanns, B. Bauer, M. Garst, and S. Trebst, *Phys. Rev. B* **91**, 155135 (2015).

[23] K. Li, S.-L. Yu, and J.-X. Li, *New J. Phys.* **17**, 043032 (2015).

[24] K. Shinjo, S. Sota, S. Yunoki, K. Totsuka, and T. Tohyama, *J. Phys. Soc. Jpn.* **85**, 114710 (2016).

[25] S. Wang, Z. Qi, B. Xi, W. Wang, S.-L. Yu, and J.-X. Li, *Phys. Rev. B* **103**, 054410 (2021).

[26] T. Dey, A. V. Mahajan, P. Khuntia, M. Baenitz, B. Koteswararao, and F. C. Chou, *Phys. Rev. B* **86**, 140405 (2012).

[27] A. Catuneanu, J. G. Rau, H.-S. Kim, and H.-Y. Kee, *Phys. Rev. B* **92**, 165108 (2015).

[28] P. A. Maksimov, Z. Zhu, S. R. White, and A. L. Chernyshev, *Phys. Rev. X* **9**, 021017 (2019); *Phys. Rev. X* **12**, 019902 (2022).

[29] P. P. Stavropoulos, D. Pereira, and H.-Y. Kee, *Phys. Rev. Lett.* **123**, 037203 (2019).

[30] D. Amoroso, P. Barone, and S. Picozzi, *Nat. Commun.* **11**, 5784 (2020).

[31] K. Riedl, D. Amoroso, S. Backes, A. Razpopov, T. P. T. Nguyen, K. Yamauchi, P. Barone, S. M. Winter, S. Picozzi, and R. Valentí, *Phys. Rev. B* **106**, 035156 (2022).

[32] K. Riedl, E. Gati, and R. Valentí, *Crystals* **12** (2022).

[33] D. J. Thouless, *Proc. Phys. Soc.* **86**, 893 (1965).

[34] K. Riedl, E. Gati, D. Zielke, S. Hartmann, O. M. Vyaselev, N. D. Kushch, H. O. Jeschke, M. Lang, R. Valentí, M. V. Kartsovnik, and S. M. Winter, *Phys. Rev. Lett.* **127**, 147204 (2021).

[35] M. Holt, B. J. Powell, and J. Merino, *Phys. Rev. B* **89**, 174415 (2014).

[36] G. Misguich, C. Lhuillier, B. Bernu, and C. Waldtmann, *Phys. Rev. B* **60**, 1064 (1999).

[37] M. S. Block, R. V. Mishmash, R. K. Kaul, D. N. Sheng, O. I. Motrunich, and M. P. A. Fisher, *Phys. Rev. Lett.* **106**, 046402 (2011).

[38] O. I. Motrunich, *Phys. Rev. B* **72**, 045105 (2005).

[39] T. Cookmeyer, J. Motruk, and J. E. Moore, *Phys. Rev. Lett.* **127**, 087201 (2021).

[40] Y. Li, T. T. Mai, M. Karaki, E. V. Jasper, K. F. Garrity, C. Lyon, D. Shaw, T. DeLazzer, A. J. Biacchi, R. L. Dally, D. M. Heligman, J. Gdanski, T. Adel, M. F. Muñoz, A. Giovannone, J. R. Simpson, K. Ross, N. Trivedi, Y. M. Lu, A. R. H. Walker, and R. V. Aguilar, *arXiv:2212.05278 (unpublished)* (2022).

[41] B. J. Kim, H. Jin, S. J. Moon, J.-Y. Kim, B.-G. Park, C. S. Leem, J. Yu, T. W. Noh, C. Kim, S.-J. Oh, J.-H. Park, V. Durairaj, G. Cao, and E. Rotenberg, *Phys. Rev. Lett.* **101**, 076402 (2008).

[42] R. D. Johnson, S. C. Williams, A. A. Haghaghirad, J. Singleton, V. Zapf, P. Manuel, I. I. Mazin, Y. Li, H. O. Jeschke, R. Valentí, and R. Coldea, *Phys. Rev. B* **92**, 235119 (2015).

[43] J. c. v. Chaloupka and G. Khaliullin, *Phys. Rev. B* **94**, 064435 (2016).

[44] K. Riedl, Y. Li, R. Valentí, and S. M. Winter, *Phys. Status Solidi B* **256**, 1800684 (2019).

[45] S. M. Winter, K. Riedl, P. A. Maksimov, A. L. Chernyshev, A. Honecker, and R. Valentí, *Nat. Commun.* **8**, 1 (2017).

[46] S. M. Winter, Y. Li, H. O. Jeschke, and R. Valentí, *Phys. Rev. B* **93**, 214431 (2016).

[47] B. Wolf, D. A. S. Kaib, A. Razpopov, S. Biswas, K. Riedl, S. M. Winter, R. Valentí, Y. Saito, S. Hartmann, E. Vinokurova, T. Doert, A. Isaeva, G. Bastien, A. U. B. Wolter,

B. Büchner, and M. Lang, *Phys. Rev. B* **106**, 134432 (2022).

[48] D. A. S. Kaib, K. Riedl, A. Razpopov, Y. Li, S. Backes, I. Mazin, and R. Valentí, *npj Quantum Mater.* **7** (2022).

[49] J. G. Rau, E. K.-H. Lee, and H.-Y. Kee, *Phys. Rev. Lett.* **112**, 077204 (2014).

[50] K. Riedl, R. Valentí, and S. M. Winter, *Nat. Commun.* **10**, 2561 (2019).

[51] L. R. Walker and R. E. Walstedt, *Phys. Rev. B* **22**, 3816 (1980).

[52] S. R. Sklan and C. L. Henley, *Phys. Rev. B* **88**, 024407 (2013).

[53] S.-H. Do, S.-Y. Park, J. Yoshitake, J. Nasu, Y. Motome, Y. Kwon, D. T. Adroja, D. J. Voneshen, K. Kim, T.-H. Jang, J.-H. Park, K.-Y. Choi, and S. Ji, *Nat. Phys.* **13**, 1079 (2017).

[54] J. G. Rau, P. A. McClarty, and R. Moessner, *Phys. Rev. Lett.* **121**, 237201 (2018).

[55] A. Banerjee, J. Yan, J. Knolle, C. A. Bridges, M. B. Stone, M. D. Lumsden, D. G. Mandrus, D. A. Tennant, R. Moessner, and S. E. Nagler, *Science* **356**, 1055 (2017).

[56] P. Bhattacharyya, N. A. Bogdanov, S. Nishimoto, S. D. Wilson, and L. Hozoi, *arXiv:2212.09365 (unpublished)* (2022).

[57] K. Koepernik and H. Eschrig, *Phys. Rev. B* **59**, 1743 (1999).

[58] J. P. Perdew, K. Burke, and M. Ernzerhof, *Phys. Rev. Lett.* **78**, 1396 (1997).

[59] E. R. Ylvisaker, W. E. Pickett, and K. Koepernik, *Phys. Rev. B* **79**, 035103 (2009).

[60] P. Blaha, K. Schwarz, G. K. H. Madsen, D. Kvasnicka, J. Luitz, R. Laskowsk, F. Tran, L. Marks, and L. Marks, *WIEN2k: An Augmented Plane Wave Plus Local Orbitals Program for Calculating Crystal Properties* (Techn. Universität, 2019).

[61] V. I. Anisimov, I. V. Solovyev, M. A. Korotin, M. T. Czyżyk, and G. A. Sawatzky, *Phys. Rev. B* **48**, 16929 (1993).

[62] A. I. Liechtenstein, V. I. Anisimov, and J. Zaanen, *Phys. Rev. B* **52**, R5467 (1995).

[63] F. Neese, *Wiley Interdiscip. Rev. Comput. Mol. Sci.* **2**, 73 (2012); *WIREs Comput. Mol. Sci.* **12**, e1606 (2022); *J. Chem. Phys.* **122**, 034107 (2005).

[64] V. Barone and M. Cossi, *J. Chem. Phys. A* **102**, 1995 (1998).

[65] F. Aryasetiawan, M. Imada, A. Georges, G. Kotliar, S. Biermann, and A. I. Lichtenstein, *Phys. Rev. B* **70**, 195104 (2004).

[66] F. Aryasetiawan, K. Karlsson, O. Jepsen, and U. Schönberger, *Phys. Rev. B* **74**, 125106 (2006).

[67] H. Jiang, R. I. Gómez-Abal, X. Li, C. Meisenbichler, C. Ambrosch-Draxl, , and M. Scheffler, *Computer Phys. Commun.* **184**, 348 (2012).

[68] J. K. Glasbrenner, I. I. Mazin, H. O. Jeschke, P. J. Hirschfeld, R. M. Fernandes, and R. Valentí, *Nat. Phys.* **11**, 953 (2015).

[69] Y. Iqbal, T. Müller, K. Riedl, J. Reuther, S. Rachel, R. Valentí, M. J. P. Gingras, R. Thomale, and H. O. Jeschke, *Phys. Rev. Materials* **1**, 071201 (2017).

[70] D. Guterding, R. Valentí, and H. O. Jeschke, *Phys. Rev. B* **94**, 125136 (2016).

[71] G. Kresse and J. Hafner, *Phys. Rev. B* **47**, 558 (1993).

[72] S. L. Dudarev, G. A. Botton, S. Y. Savrasov, C. J. Humphreys, and A. P. Sutton, *Phys. Rev. B* **57**, 1505 (1998).

[73] S. Toth and B. Lake, *J. Phys. Condens. Matter* **27**, 166002 (2015).

Supplementary Information:

A $j_{\text{eff}}=1/2$ Kitaev material on the triangular lattice: The case of NaRuO_2

Aleksandar Razpopov,¹ David A. S. Kaib,¹ Steffen Backes,^{2,3,4} Leon Balents,⁵ Stephen D. Wilson,⁶ Francesco Ferrari,¹ Kira Riedl,¹ and Roser Valentí¹

¹*Institut für Theoretische Physik, Goethe-Universität, 60438 Frankfurt am Main, Germany*

²*Research Center for Advanced Science and Technology, University of Tokyo, Komaba, Tokyo 153-8904, Japan*

³*Center for Emergent Matter Science, RIKEN, Wako, Saitama 351-0198, Japan*

⁴*CPHT, CNRS, École polytechnique, Institut Polytechnique de Paris, 91120 Palaiseau, France*

⁵*Kavli Institute for Theoretical Physics, University of California, Santa Barbara, California 93106, USA*

⁶*Materials Department, University of California, Santa Barbara, California 93106-5050, USA*

(Dated: January 18, 2023)

Supplementary Note 1: Relation of j_{eff} and j states

In general, the relativistic basis of d block electrons consists of $j = \{5/2, 3/2\}$ states. However, in an octahedral environment, the $e_g = \{x^2-y^2, z^2\}$ orbitals may be high enough in energy, to make a description in terms of $j_{\text{eff}} = \{3/2, 1/2\}$ states more appropriate [1, 2]. Here, we revisit briefly the relation between these two representations.

The $j = 3/2$ states consist of a sum of $j_{\text{eff}} = 3/2$ states and e_g states, as evident from the following expressions:

$$|\frac{3}{2}, +\frac{3}{2}\rangle = +\sqrt{\frac{3}{5}}i|\frac{3}{2}, -\frac{1}{2}\rangle_{\text{eff}} + \sqrt{\frac{2}{5}}|x^2-y^2, \downarrow\rangle \quad (1)$$

$$|\frac{3}{2}, +\frac{1}{2}\rangle = -\sqrt{\frac{3}{5}}i|\frac{3}{2}, -\frac{3}{2}\rangle_{\text{eff}} - \sqrt{\frac{2}{5}}|z^2, \uparrow\rangle \quad (2)$$

$$|\frac{3}{2}, -\frac{1}{2}\rangle = -\sqrt{\frac{3}{5}}i|\frac{3}{2}, +\frac{3}{2}\rangle_{\text{eff}} + \sqrt{\frac{2}{5}}|z^2, \downarrow\rangle \quad (3)$$

$$|\frac{3}{2}, -\frac{3}{2}\rangle = +\sqrt{\frac{3}{5}}i|\frac{3}{2}, +\frac{1}{2}\rangle_{\text{eff}} - \sqrt{\frac{2}{5}}|x^2-y^2, \uparrow\rangle \quad (4)$$

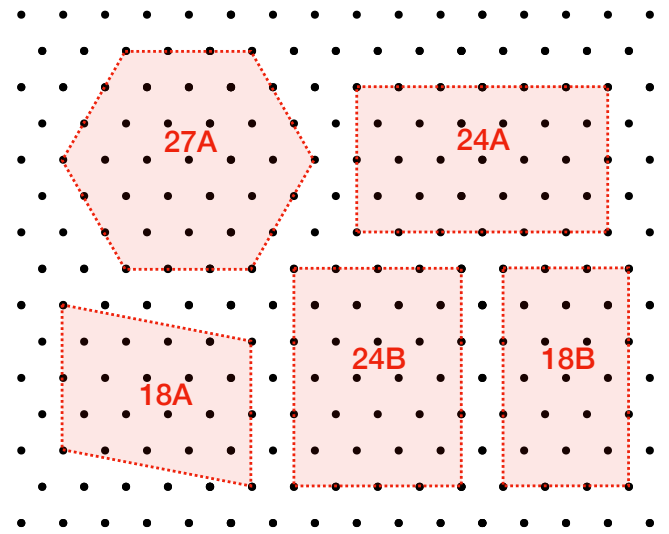
In contrast, the information about $j_{\text{eff}} = 1/2$ states is included in a linear combination of $j = 5/2$ states:

$$|\frac{1}{2}, +\frac{1}{2}\rangle_{\text{eff}} = \sqrt{\frac{1}{6}}i|\frac{5}{2}, +\frac{5}{2}\rangle - \sqrt{\frac{5}{6}}i|\frac{5}{2}, -\frac{3}{2}\rangle \quad (5)$$

$$|\frac{1}{2}, -\frac{1}{2}\rangle_{\text{eff}} = \sqrt{\frac{1}{6}}i|\frac{5}{2}, -\frac{5}{2}\rangle - \sqrt{\frac{5}{6}}i|\frac{5}{2}, +\frac{3}{2}\rangle \quad (6)$$

Supplementary Note 2: Bilinear Hamiltonian in the crystallographic reference frame

In the main text the bilinear Hamiltonian is given in cubic coordinates (shown in Fig. 1b of the main text). Another possible spin coordinate frame, dubbed *crystallographic* frame, is the one in which spin coordinates $(\tilde{S}^x, \tilde{S}^y, \tilde{S}^z)$ co-align with crystallographic (a, b^*, c) directions, as used e.g. in Ref. [3] (and labelled as “cryst” in the following). In the latter framework, focusing on nearest-neighbor bonds, for which anisotropic interactions are relevant, the Hamiltonian

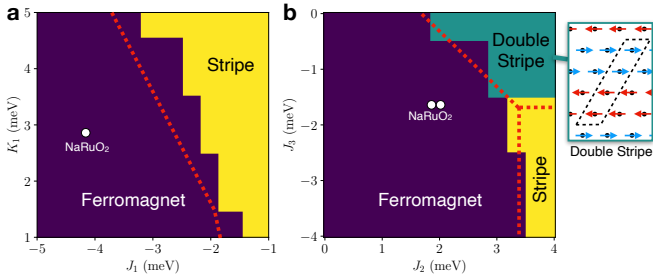


Supplementary Figure 1. **Finite-size clusters used in exact diagonalization calculations.** Dotted lines represent periodic boundaries. Respective number of sites is denoted within each cluster.

reads

$$\begin{aligned} \mathcal{H}_2^{\text{cryst}} = & \sum_{\langle i,j \rangle} \{ J^{\text{cryst}} (\tilde{S}_i^x \tilde{S}_j^x + \tilde{S}_i^y \tilde{S}_j^y + \Delta^{\text{cryst}} \tilde{S}_i^z \tilde{S}_j^z) \\ & + 2 J_{\pm, \pm}^{\text{cryst}} [(\tilde{S}_i^x \tilde{S}_j^x - \tilde{S}_i^y \tilde{S}_j^y) c_\alpha - (\tilde{S}_i^x \tilde{S}_j^y + \tilde{S}_i^y \tilde{S}_j^x) s_\alpha] \\ & + J_{z, \pm}^{\text{cryst}} [(\tilde{S}_i^y \tilde{S}_j^z + \tilde{S}_i^z \tilde{S}_j^y) c_\alpha - (\tilde{S}_i^x \tilde{S}_j^z + \tilde{S}_i^z \tilde{S}_j^x) s_\alpha] \}, \end{aligned} \quad (7)$$

where $c_\alpha = \cos(\varphi_\alpha)$, $s_\alpha = \sin(\varphi_\alpha)$ and $\varphi_\alpha = (0, \frac{2\pi}{3}, -\frac{2\pi}{3})$ for X_1 -, Y_1 - and Z_1 -bonds, respectively [3]. In the crystallographic reference frame, the nearest-neighbor couplings of NaRuO_2 are $(J^{\text{cryst}}, \Delta^{\text{cryst}}, J_{\pm, \pm}^{\text{cryst}}, J_{z, \pm}^{\text{cryst}}) = (-5.97, -0.39, -2.59, -1.65)$ meV, where we note the unusual negative sign of the XXZ anisotropy parameter Δ^{cryst} .



Supplementary Figure 2. Phases of the magnetic bilinear Hamiltonian around the ab-initio estimate for NaRuO_2 . Phase diagram of the (in-plane) bilinear Hamiltonian \mathcal{H}_2 when tuning **a** the nearest-neighbors interactions J_1 and K_1 , **b** the longer-range couplings J_2 and J_3 . The remaining parameters are fixed and equal to the ones given in Fig. 1d of the main text. The white circles indicate the *ab-initio* derived Hamiltonian for NaRuO_2 . The colormap shows the phases obtained by ED calculations (on a coarse finite grid of values, cluster 24A), while the red dashed lines mark the classical phase boundaries. The inset on the right of **b** shows the periodic arrangement of the spins in the double stripe phase (the magnetic unit cell is marked with dashed lines).

Supplementary Note 3: Details of Exact Diagonalization calculations

In Supplementary Figure 1 we show the various clusters employed in exact diagonalization (ED) calculations. The neutron scattering intensity shown in Fig. 3b of the main text combines results from different momenta allowed on different clusters. For momenta that exist on multiple clusters, the averaged intensity from all such clusters is shown.

Supplementary Note 4: Perturbations to magnetic Hamiltonian

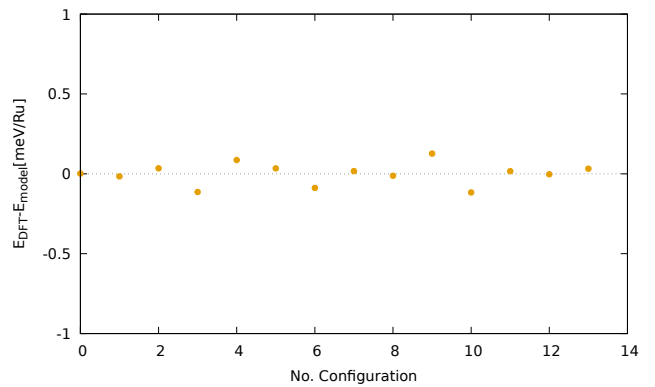
As discussed in the main text, the magnetic Hamiltonian derived in this study yields a ferromagnetic (FM) ordered ground state. However, different experimental samples might have certain variations in their lattice structure [4], changing their magnetic couplings. Furthermore, the *ab-initio* calculation of the magnetic Hamiltonian depends on input parameters and approximations to some degree. It is therefore interesting to consider how stable the FM ground state of the model is against modest perturbations. We here consider for simplicity only our bilinear model \mathcal{H}_2 with in-plane interactions. This precise model is not captured by existing phase diagrams [3, 5] due to the presence of finite Γ' , negative Δ^{cryst} (see Supplementary Note 2), and finite further-neighbor J_2, J_3 interactions. We therefore perform various classical energy minimization and ED calculations perturbing around the *ab-initio* derived Hamiltonian. Two phase diagrams are shown in Supplementary Figure 2, in which either K_1 and J_1 , or J_2 and J_3 , are tuned around the NaRuO_2 in-plane bilinear model (marked by the white circle). In all cases, changes of multiple meV to the pa-

rameters in the Hamiltonian are needed to destabilize the ferromagnetic state. This amount of variation exceeds the typical degree of uncertainty expected in the *ab-initio* calculations, supporting the assessment of a pristine NaRuO_2 compound to be ferromagnetic. Interestingly, we note that a “double-stripe” magnetic order is relatively proximate to the NaRuO_2 model. The “double-stripe” order resembles the “stripe” phase, but with a doubled unit cell size, as shown in the inset of Supplementary Figure 2.

We also consider slight variations in the U and J_H (Hund’s coupling) parameters away from the cRPA-computed values, which are used in the projED derivation for the magnetic Hamiltonians. However, modest variations of these parameters (e.g., ± 0.1 eV for J_H and ± 1 eV for U) still lead to magnetic Hamiltonians with a FM ground state. With decreasing U , the (anisotropic) ring exchange interaction tends to increase, however not enough to destabilize the FM order for realistic U and J_H values.

Supplementary Note 5: Quality of total energy mapping analysis

To quantify the quality of the total energy mapping analysis we consider the difference between the energy of the DFT (GGA+U) calculation and the one provided by the fitting magnetic model. The result is shown in Supplementary Figure 3 for each configuration (labelled by a number). Small deviations between the model calculations and DFT calculations are expected to be accounted for by longer range interactions which are not considered in the model. The small total energy difference (0.049 meV/Ru per configuration) suggests that all relevant exchange couplings are included in the magnetic model.



Supplementary Figure 3. Quality of the total energy mapping analysis. The difference between the total DFT (GGA+U) energy and the one from the magnetic model is shown as a function of the different magnetic configurations, labelled by an integer number.

- [1] B. J. Kim, H. Jin, S. J. Moon, J.-Y. Kim, B.-G. Park, C. S. Leem, J. Yu, T. W. Noh, C. Kim, S.-J. Oh, J.-H. Park, V. Durairaj, G. Cao, and E. Rotenberg, *Phys. Rev. Lett.* **101**, 076402 (2008).
- [2] S. M. Winter, A. A. Tsirlin, M. Daghofer, J. van den Brink, Y. Singh, P. Gegenwart, and R. Valentí, *J. Phys. Condens. Matter* **29**, 493002 (2017).
- [3] P. A. Maksimov, Z. Zhu, S. R. White, and A. L. Chernyshev, *Phys. Rev. X* **9**, 021017 (2019); *Phys. Rev. X* **12**, 019902 (2022).
- [4] B. Ortiz, P. Sarte, A. H. Avidor, A. Hay, E. Kenney, A. Kolesnikov, A. Aczel, C. Brown, C. Wang, M. Graf, R. Se-shadri, L. Balents, and S. Wilson, *Preprint available at Research Square* (2022).
- [5] S. Wang, Z. Qi, B. Xi, W. Wang, S.-L. Yu, and J.-X. Li, *Phys. Rev. B* **103**, 054410 (2021).